Coupled Systems Mechanics, *Vol. 12, No. 5 (2023) 409-418*
https://doi.org/10.12989/csm.2023.12.5.409

A coupled simulation of parametric porous microstructure and stress-strain behavior in mechanical components under variable cyclic loads

Domen Šeruga*, Jernej Klemenc[a], Simon Oman[b] and Marko Nagode[a]

Faculty of Mechanical Engineering, University of Ljubljana, Aškerčeva 6, 1000 Ljubljana, Slovenia

(Received March 31, 2023, Revised May 2, 2023, Accepted May 17, 2023)

Abstract. A coupled algorithm is proposed which first considers the creation of porous structure of the material and then the simulations of response of mechanical components with porous structure to a variable load history. The simulations are carried out by the Prandtl operator approach in the finite element method (FEM) which enables structural simulations of mechanical components subjected to variable thermomechanical loads. Temperature-dependent material properties and multilinear kinematic hardening of the material can be taken into account by this approach. Several simulations are then performed for a tensile-compressive specimen made of a generic porous structure and mechanical properties of Aluminium alloy AlSi9Cu3. Variable mechanical load history has been applied to the specimens under constant temperature conditions. Comparison of the simulation results shows a considerable elastoplastic stress-strain response in the vicinity of pores whilst the surface of the gauge-length of the specimen remains in the elastic region of the material. Moreover, the distribution of the pore sizes seems more influential to the stress-strain field during the loading than their radial position in the gauge-length.

Keywords: cyclic loading; elastoplasticity; finite element analysis; porous structure

1. Introduction

Mechanical components operate in complex conditions. The joint effects of components' use and operating environment coupled by their mechanical characteristics, e.g., shape, size and material, determine their availability during service life. The development of new products hence requires several development evaluations to verify the project requirements. These evaluations include structural behavior, durability prediction, reliability, and safety analyses among others (Liao *et al.* 2022, Bartošák 2021, Šeruga *et al.* 2014, Gharib *et al.* 2022). The listed analyses are commonly based on the coupled consideration of the material properties with the thermomechanical influences from use and environment (Šeruga *et al.* 2014). The resulting stress-strain behavior of the mechanical component is gained numerically in the early stages of the R&D

*Corresponding author, Associate Professor, E-mail: domen.seruga@fs.uni-lj.si
[a]Full Professor
[b]Assistant Professor

http://www.techno-press.org/?journal=csm&subpage=8 ISSN: 2234-2184 (Print), 2234-2192 (Online)

process or experimentally in later stages (Imamovic *et al.* 2022, Bartošák 2021, Hajdo *et al.* 2020, Šeruga *et al.* 2014, Pagliaro *et al.* 2020). The accuracy of the simulations depends on the considered level of details, either regarding the material properties or the typical use and environmental conditions. The numerical models used in the finite element analysis (FEA), where stress-strain calculations are commonly carried out, can be set either as to (i) use an ideal volume with material properties which resemble the material peculiarities, e.g., pores in the microstructure as a consequence of the manufacturing process, or (ii) use a realistic volume with the imperfections modelled as they appear (Polatov *et al.* 2020, Zouambi *et al.* 2014, Ghasemi *et al.* 2022, Li *et al.* 2019). In both cases, a coupled analysis between the microstructure and the stress-strain response can be performed providing the macroscopic behavior of the component during loading. However, the latter option offers an additional insight into the behavior of the internal structure. With other words, the influence of the pore distribution due to the manufacturing process can be studied and understood if a detailed model is created. Several methods of how to introduce the pores into the finite element model have been reported. They can be divided into explicit and implicit pore geometry modelling, and stochastic methods. On one hand, explicit pore geometry modelling involves direct incorporation of the pore geometry into the finite element model, e.g., Tomažinčič *et al.* (2021), Zouambi *et al.* (2014) or Bižal *et al.* (2015). Implicit pore modelling, on the other hand, reflects the effect of the pores in the values of the material parameters whereas the finite element mesh is modelled without pores, e.g., Osmond *et al.* (2018). Stochastic methods involve generating random pores within the model and simulating their effects on the material properties, e.g., Pang and Yuan (2020). The choice of pore modelling approach depends on the specific application and the accuracy required in the simulation. Additionally, accurate characterization of the pore geometry and material properties is critical in developing a reliable finite element model which can effectively simulate the behavior of the material (Tomažinčič and Klemenc 2022).

As variable cyclic loads cause load-history-dependent stress-strain response in the material, the simulations must consider these phenomena, too. However, simulations of cyclic phenomena on large finite element models usually involve high computational requirements, therefore a time-efficient method can aid to reduce the processing times during the solution of the problem. The Prandtl operator approach therefore seems a valuable choice as it enables simulations of a cyclic stress-strain response due to variable thermomechanical loads of mechanical components. Its main advantages are high computational power and a small number of required material parameters to carry out the simulations (Nagode and Zingsheim 2004, Nagode and Fajdiga 2007). It has recently been implemented into the finite element method (FEM) as a user-material subroutine (UMAT) and enables temperature-dependent elastoplastic material properties with consideration of multilinear kinematic hardening either within the elastic predictor–plastic corrector iteration routine (Šeruga and Nagode 2019) or as a closed-form solution (Nagode *et al.* 2021). So far, it has been tested on simple structures (Nagode *et al.* 2021), a pipe-bend (Šeruga *et al.* 2022a) and a perforated plate (Šeruga *et al.* 2022b).

Here we propose the extension of the Prandtl operator approach into a coupled algorithm which considers first the creation of porous structure of the material and then the simulations of response of mechanical components with porous structure to a variable load history. The method of the algorithm initially allows for statistical modelling of the size and the position of the pores by a random distribution, then provides the implementation of the results of the statistical step into the geometry of the mechanical component and finally carries out the simulations of the stress-strain response of the component subjected to a variable loading history.

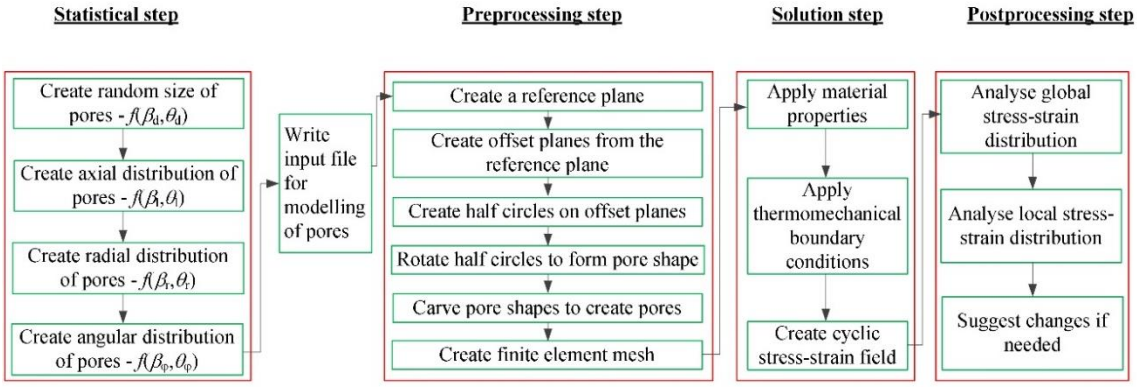

Fig. 1 Algorithm for creation of the realistic virtual manufacturing-process-influenced finite element mesh and solution of the stress-strain field during variable loading

2. Method

The first integral part of the method is an autogenous generic algorithm based on either a uniform distribution $U(x)$ or a two-parameter Weibull distribution $W(x)$ which join a theoretical distribution of the pores with an ideal CAD model and then convert them into a realistic virtual manufacturing process-influenced finite element mesh of the mechanical component. The size and the spatial position of a single pore are thus given in terms of the probability density functions as

$$f(x) = \begin{cases} U(x); & x = d, l, r, \varphi \quad \vee \\ W(x) = \left(\frac{\beta_x}{\theta_x}\right)\left(\frac{x}{\theta_x}\right)^{(\beta_x - 1)} e^{-\left(\frac{x}{\theta_x}\right)^{\beta_x}}; & x = d, l, r, \varphi. \end{cases} \tag{1}$$

Variables d, l, r and φ stand for the diameter of the pores, the axial distance, the radius in the gauge part of the specimen and the angle in the gauge section, respectively. Since every pore p_i (d, l, r, φ); i =1, ..., m is created as an intersection between the geometric primitive and the model, incremental building of the final model is utilized by a loop iterating through the number of pores m (Fig. 1)

$$p_i(d, l, r, \varphi) = \begin{cases} \int_0^{x_i} U(x)dx; & x = d, l, r, \varphi;\ i = 1, \ldots, m \quad \vee \\ \int_0^{x_i} W(x)dx; & x = d, l, r, \varphi;\ i = 1, \ldots, m. \end{cases} \tag{2}$$

The biggest advantage of such modelling of pores is a parametric representation of the pores which allows for potential corrections of either their size or positions (if required) after the inspection of the model. Next, meshing with finite elements creates a numerical model with geometric features of the manufacturing process (pores).

The second integral part of the method is a closed-form solution for the determination of the stress-strain field during variable loading of the virtual mechanical component. The closed form ensures a high computational speed which is crucial for complex finite element models. Specifically, observing the integration-point level in a finite-element model, the stress-tensor increment $\Delta\sigma_{ij}$ can be modelled for a given strain-tensor increment $\Delta\varepsilon_{ij}$. The strain-tensor increments are supplied in steps k=1, ..., n. If constant temperature is assumed, the connection between the stress-tensor and the strain-tensor increments can then be written as

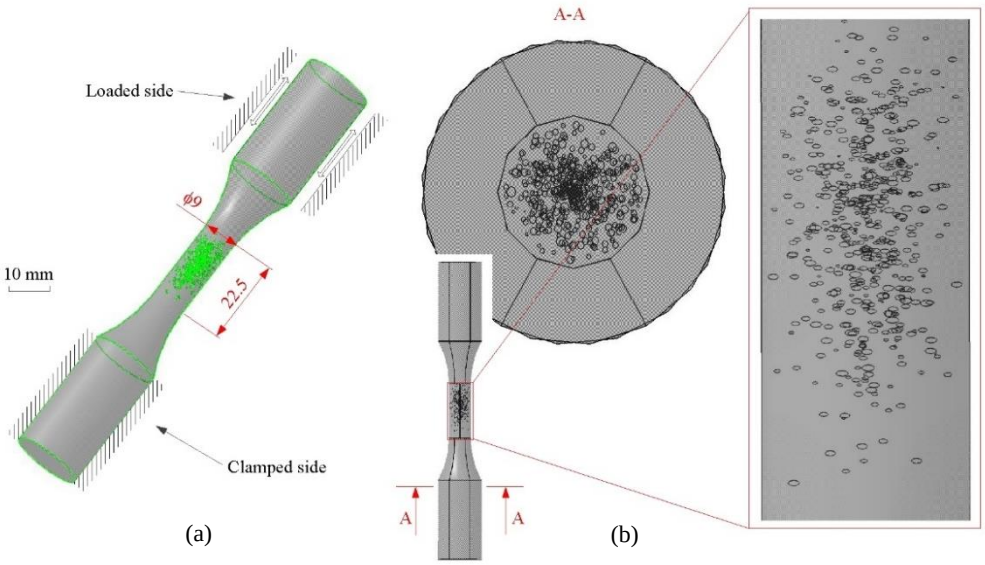

Fig. 2 (a) Specimen 1 and (b) controlled distribution of pores in the gauge-length for specimen 1

$$\Delta\sigma_{ij} = 2\mu^*\Delta\varepsilon_{ij} + \lambda^*\Delta\varepsilon_{kk}\delta_{ij}, \tag{3}$$

where μ^* and λ^* stand for elastoplastic Lamé constants

$$\mu^* = \frac{\Delta\rho_s}{\Delta\rho_e} \text{ and } \lambda^* = \frac{E}{3(1-2\nu)} - \frac{2}{3}\mu^*, \tag{4}$$

whilst E and ν are Young modulus and Poisson ratio of the material. The mechanical radial stress increment in the deviatoric plane $\Delta\rho_s$ can be expressed in a form of a Prandtl operator type for constant temperature conditions as

$$\Delta\rho_s = \sum_{l=1}^{n_q} \alpha_l \Delta\rho_{(e)l}, \tag{5}$$

where α_l, $\Delta\rho_{(e)l}$ and n_q stand for Prandtl densities, radial back-strain increments and the number of the Prandtl-type spring-slider segments, respectively. A detailed description of the calculation procedure using the FEM-implemented Prandtl operator approach can be found in Nagode *et al.* (2021).

Reliability calculation of the material and determination of confidence intervals can be achieved by a straightforward extension of the method. Bootstrapping using a redistribution of pores with unchanged distribution parameters followed by re-meshing and recalculation of the stress-strain response can be utilized for this purpose.

3. Results and discussion

Several porous tensile-compressive specimens with the gauge-length dimensions of 22.5×9 mm have been created for validation purposes in this study (Figs. 2, 3, 4 and 5). First, the pores have been prepared for the ideal geometry of the specimen using the presented algorithm based on a uniform radial distribution for one specimen (Fig. 2). Additionally, four combinations of pore sizes

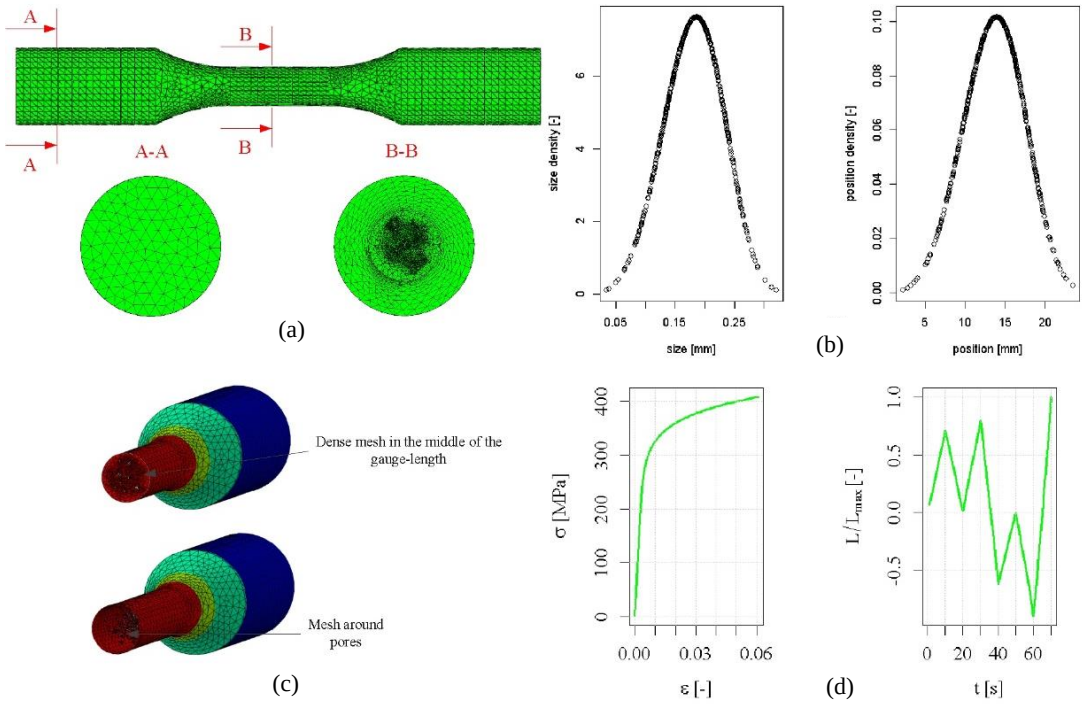

Fig. 3 (a) Mesh of specimen 1, (b) size and position distribution of the pores in the axial direction of the gauge-length in specimen 1 (uniform radial distribution of pores was used in this case), (c) detailed mesh around the pores for specimen 1 and (d) material properties of the bulk material and the variable amplitude loading for all the specimens

Table 1 Elastic modulus E, Ramberg-Osgood parameters K' and n' and proportional limit stress σ_p for Aluminium alloy AlSi9Cu3 (Bižal *et al.* 2015, Tomažinčič and Klemenc 2022)

T [°C]	E [MPa]	K' [MPa]	n' [-]	σ_p [MPa]
23	70000	542	0.098	178

and radial positions have been set using the two-parameter Weibull distribution as shown in Figs. 4 and 5. The axial distribution of the pores has been set by the same two-parameter Weibull distribution for all the specimens (Fig. 3(b)). The resulting finite element meshes consisted of 120770, 98506, 110244, 98937 and 97291 nodes, and 706695, 573397, 638871 575156, 567313 C3D4 structural elements for specimens 1 to 5, respectively.

Apart from the elastic modulus, which was set to 70000 MPa, the material properties of the bulk material have been chosen according to Bižal *et al.* (2015) and Tomažinčič and Klemenc (2022). The uniaxial tensile-compressive cyclic stress-strain curve is given in Fig. 3(d) and the material properties of the bulk material are listed in Table 1.

One side of the specimens has been clamped and the other side has been mechanically loaded by a variable displacement-controlled loading as depicted in Fig. 2(a). The complete mechanical load history of the specimen, applied in seven load steps, is graphically presented in Fig. 3(d). Every load step has been further divided into automatically controlled sub-steps to ensure the convergence of the mechanical solution. Finally, a control point on specimen 1 has been chosen for

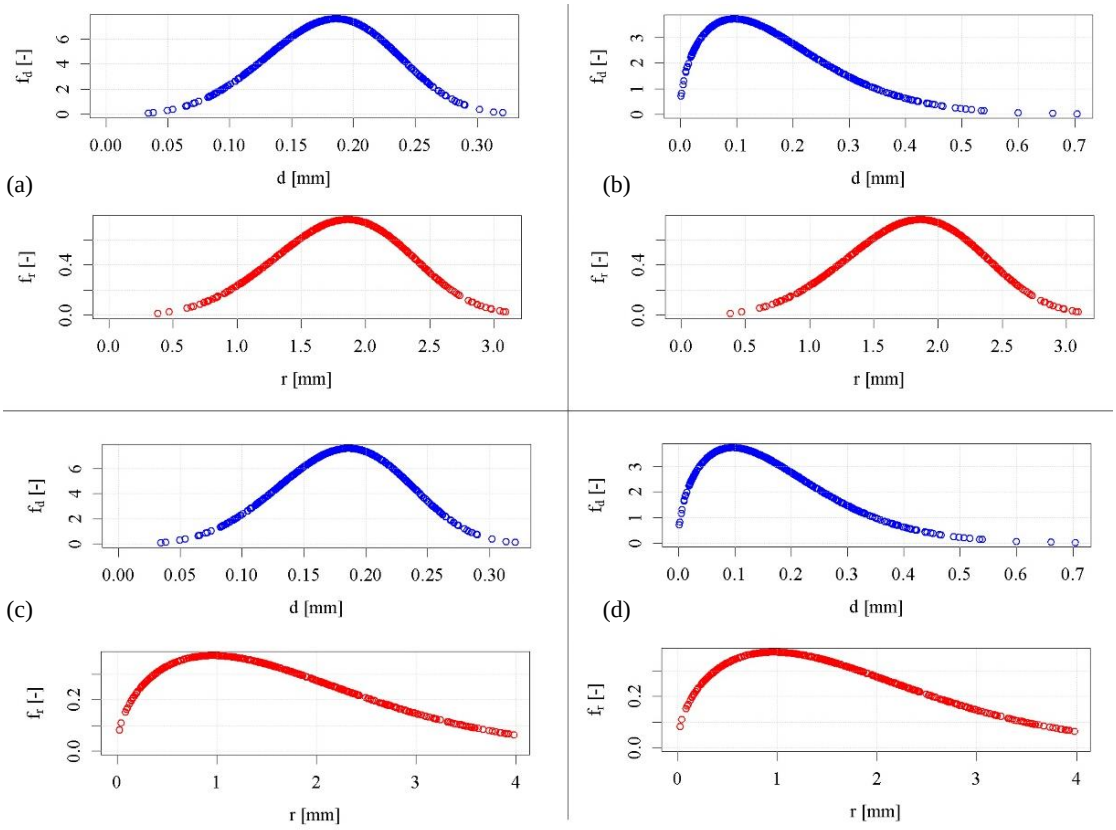

Fig. 4 Distributions of pore size and radial positions in: a) specimen 2, b) specimen 3, c) specimen 4 and d) specimen 5

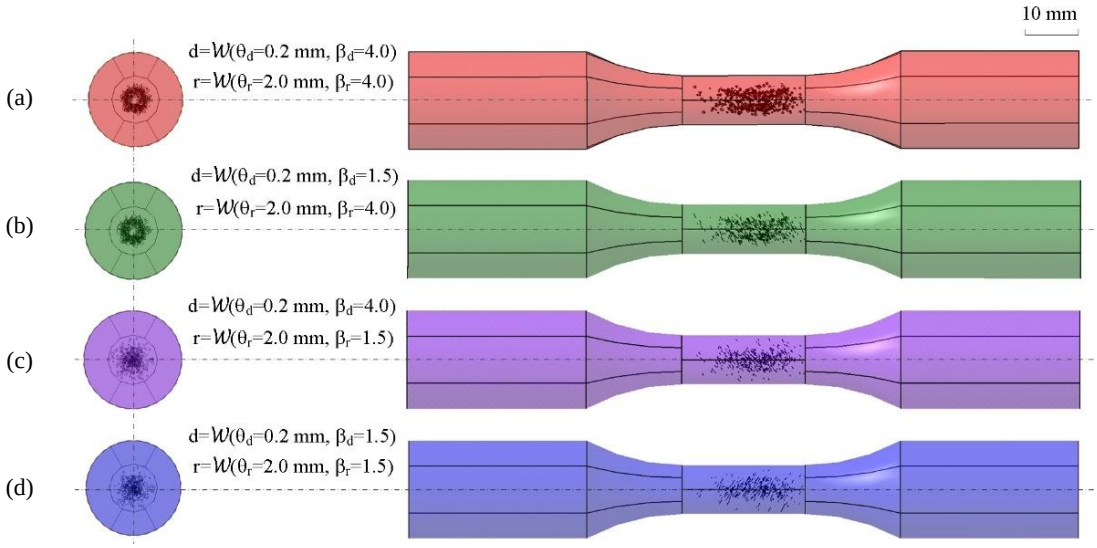

Fig. 5 Geometry after the completion of the preprocessing step of the algorithm: (a) specimen 2, (b) specimen 3, (c) specimen 4 and (d) specimen 5

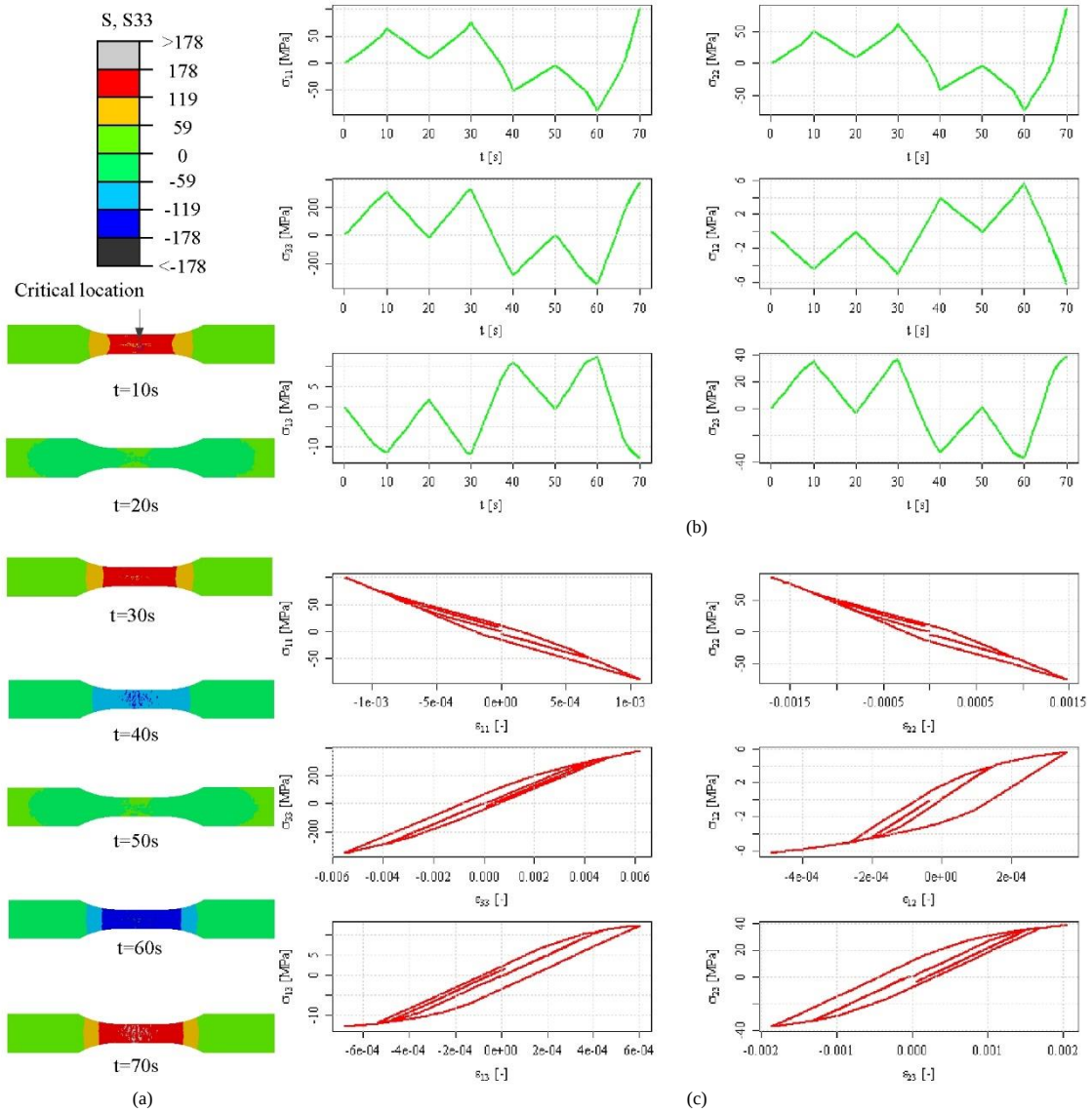

Fig. 6 (a) Simulation results for the middle plane of specimen 1. Critical location is pointed out. (b) Stress-tensor simulation results for the critical location on specimen 1. (c) Stress-strain tensor results for the critical location on specimen 1

analysis of the stress-strain simulation results.

The simulation results for specimen 1 are depicted in Fig. 6 and for specimens 2-5 in Fig. 7. The analysis of specimen 1 provides scrutiny regarding the application of the Prandtl operator approach to carry out the coupled simulations of porous microstructure and variable loading of mechanical components. Furthermore, the examination of the stress-strain results in specimens 2-5 delivers the influence of the variation in microstructure depending on the pore size and position distributions.

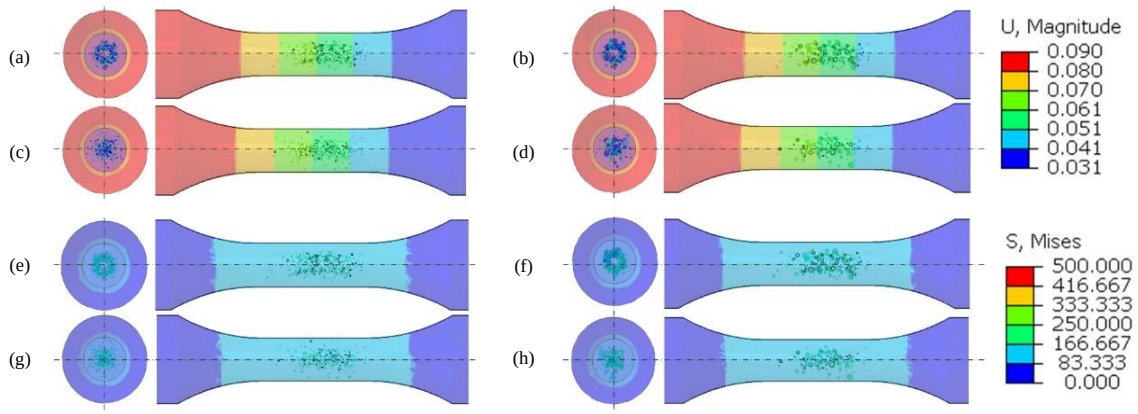

Fig. 7 Displacement simulation results after 10 s for (a) specimen 2, (b) specimen 3, (c) specimen 4 and (d) specimen 5; and von Mises stress simulation results after 10 s for (e) specimen 2, (f) specimen 3, (g) specimen 4 and (h) specimen 5

Initially, it can be noticed that for the given loads, the surface of the gauge-length remains in the elastic region of the material, whilst an elastoplastic stress-strain response can be observed around the pores (Fig. 6(a)). Moreover, despite the uniaxial loading of the specimen a multiaxial response appears in the vicinity of the pores which is clearly noticeable for the chosen control point (critical location) in Fig. 6(b) and 6(c). A nonlinear stress-time response is observed due to the nonlinear material behaviour beyond the plastic limit of the material (Fig. 6(b)), although the loading of the specimen is applied linearly (Fig. 3(d)). Specifically, the simulation using the Prandtl operator approach considers kinematic hardening of the material and memory rules during the application of the variable amplitude loading which can be seen in the modelled stress-strain hysteresis loops (Fig. 6(c)).

Furthermore, comparison of the various pore distributions reveals that higher values of both the pore size and radial positions will appear in the specimen for lower values of the Weibull shape parameter β (Figs. 4 and 5). Importantly, the size parameter θ has been kept constant for all the specimens 2-5. The influence of this fact can thus be clearly seen in displacement and stress distributions across the cross-sections as depicted in Fig. 7. The simulations show that favourable von Mises stresses in the whole gauge-length are achieved for specimen 5 (374 MPa in step 1), whereas the most detrimental effect due to the simulated porous microstructure is observed for specimen 2 (503 MPa in step 1). Specimen 3 reached the second highest von Mises stress (403 MPa in step 1) and specimen 4 with 379 MPa was just before specimen 5 (361 MPa). The visual comparison of specimen 2-5 cross-sections in step 1 is given in Fig. 7. Observing the pore distributions in Fig. 4 and the values of the stresses in the gauge cross-section therefore suggests that the pore size distribution has a slightly greater effect on the mechanically loaded material (drop from 503 MPa in Fig. 7(e) to 379 MPa in Fig. 7(g)) than the position distribution (drop from 503 MPa in Fig. 7(e) to 403 MPa in Fig. 7(f)).

5. Conclusions

The paper has investigated a stress-strain simulation of a complex model using the coupled

consideration of the porous microstructure and the FEM-implemented Prandtl operator approach. The results show an elastoplastic response in the vicinity of the pores in the gauge-length whilst the macroscopic response of the specimen remains in the elastic region of the material. Furthermore, a multiaxial stress-strain state appears around the pores although the loading of the specimen is uniaxial. Importantly, the response can be simulated for variable amplitude loading with consideration of multilinear kinematic hardening. Using a two-parameter Weibull distribution for modelling of pore sizes and their radial position in the gauge-length, the former turned out to be to some extent more influential in respect with induced stress field in the material than their radial position.

Acknowledgments

The authors acknowledge financial support from the Slovenian Research Agency (research core funding No. P2-0182 entitled Development Evaluation).

References

Bartošák, M. (2021), "Constitutive modelling for isothermal low-cycle fatigue and fatigue-creep of a martensitic steel", *Mech. Mater.*, **162**, 104032. https://doi.org/10.1016/j.mechmat.2021.104032.

Bižal, A., Klemenc, J. and Fajdiga, M. (2015), "Modelling the fatigue life reduction of anAlSi9Cu3 alloy caused by macro-porosity", *Eng. Comput.*, **31**(2), 259-269. https://doi.org/10.1007/s00366-013-0345-7.

Gharib, M., Ceccarelli, A., Lollini, P. and Bondavalli, A. (2022), "A cyber-physical-social approach for engineering functional safety requirements for automotive systems", *J. Syst. Softw.*, **189**, 111310. https://doi.org/10.1016/j.jss.2022.111310.

Ghasemi, M., Falahatgar, S. and Mosto, T. (2022), "Mechanical and thermomechanical mesoscale analysis of multiple surface cracks in ceramic coatings based on the dem-fem coupling method", *Int. J. Solid. Struct.*, **236-237**, 111336. https://doi.org/10.1016/j.ijsolstr.2021.111336.

Hajdo, E., Ibrahimbegovic, A. and Dolarevic, S. (2020), "Buckling analysis of complex structures with refined model built of frame and shell finite elements", *Couple. Syst. Mech.*, **9**(1), 29-46. https://doi.org/10.12989/csm.2020.9.1.029.

Imamovic, I., Ljukovac, S. and Ibrahimbegovic, A. (2022), "Advanced approach to design of small wind turbine support structures", *Couple. Syst. Mech.*, **11**(6), 525-542. https://doi.org/10.12989/csm.2022.11.6.525.

Li, H., Dong, S., Liu, J., Yu, Y., Wu, M. and Zhang, Z. (2019), "Finite element modeling of porous microstructures with random holes of different-shapes and sizes to predict their effective elastic behavior", *Appl. Sci.*, **9**(21), 4536. https://doi.org /10.3390/app9214536.

Liao, D., Zhu, S.P., Correia, J.A., Jesus, A.M.D., Veljkovic, M. and Berto, F. (2022), "Fatigue reliability of wind turbines: historical perspectives, recent developments and future prospects", *Renew. Energy*, **200**, 724-742. https://doi.org/10.1016/j.renene.2022.09.093.

Nagode, M. and Fajdiga, M. (2007), "Coupled elastoplasticity and viscoplasticity under thermomemechanical loading", *Fatig. Fract. Eng. Mater. Struct.*, **30**(6), 510-519. https://doi.org/10.1111/j.1460-2695.2007.01121.x.

Nagode, M. and Zingsheim, F. (2004), "An online algorithm for temperature influenced fatigue life estimation: Strain-life approach", *Int. J. Fatig.*, **26**(2), 155-161. https://doi.org/10.1016/S0142-1123(03)00107-5.

Nagode, M., Klemenc, J., Oman, S. and Šeruga, D. (2021), "A closed-form solution for temperature-dependent elastoplastic problems using the Prandtl operator approach", *Commun. Nonlin. Sci. Numer.*

Simul., **99**, 105839. https://doi.org/10.1016/j.cnsns.2021.105839.
Osmond, P., Le, V.D., Morel, F., Bellett, D. and Saintier, N. (2018), "Effect of porosity on the fatigue strength of cast aluminium alloys: from the specimen to the structure", *Procedia Eng.*, **213**, 630-643. https://doi.org/10.1016/j.proeng.2018.02.059.
Pagliaro, S., Aloisio, A., Alaggio, R. and Egidio, A.D. (2020), "Rigid block coupled with a 2 d.o.f. system: Numerical and experimental investigation", *Couple. Syst. Mech.*, **9**(6), 539-561. https://doi.org/10.12989/csm.2020.9.6.539.
Pang, K. and Yuan, H. (2020), "Fatigue life assessment of a porous casting nickel-based superalloy based on fracture mechanics methodology", *Int. J. Fatig.*, **136**, 105575. https://doi.org/10.1016/j.ijfatigue.2020.105575.
Polatov, A.M., Khaldjigitov, A.A. and Ikramov, A.M. (2020), "Algorithm of solving the problem of small elastoplastic deformation of fiber composites by FEM", *Couple. Syst. Mech.*, **5**, 305-321. https://doi.org/10.12989/acd.2020.5.3.305.
Šeruga, D. and Nagode, M. (2019), "A new approach to finite element modelling of cyclic thermomechanical stress-strain responses", *Int. J. Mech. Sci.*, **164**, 105139. https://doi.org/10.1016/j.ijmecsci.2019.105139.
Šeruga, D., Hansenne, E., Haesen, V. and Nagode, M. (2014), "Durability prediction of EN 1.4512 exhaust mufflers under thermomechanical loading", *Int. J. Mech. Sci.*, **84**, 199-207. https://doi.org/10.1016/j.ijmecsci.2014.04.004.
Šeruga, D., Klemenc, J., Oman, S. and Nagode, M. (2022a), "Elastoplastic response of a pipe bend using Prandtl operator approach in a finite element analysis", *Procedia Struct. Integr.*, **35**, 150-158. https://doi.org/10.1016/j.prostr.2021.12.059.
Šeruga, D., Klemenc, J., Oman, S. and Nagode, M. (2022b), "Structural finite element analysis using material model with prandtl operator approach", *LCF9-Ninth International Conference on Low Cycle Fatigue*, https://doi.org/10.48447/LCF9-2022-050.
Tomažinčič, D. and Klemenc, J. (2022), "Estimate of Coffin-Manson curve shift for the porous alloy AlSi9Cu3 based on numerical simulations of a porous material carried out by using the Taguchi array", *Mater.*, **15**(6), 2269. https://doi.org/10.3390/ma15062269.
Tomažinčič, D., Borovinšek, M., Ren, Z. and Klemenc, J. (2021), "Improved prediction of low-cycle fatigue life for high-pressure die-cast aluminium alloy AlSi9Cu3 with significant porosity", *Int. J. Fatig.*, **144**, 106061. https://doi.org/10.1016/j.ijfatigue.2020.106061.
Zouambi, L., Serier, B. and Benamara, N. (2014), "Effect of cavity-defects interaction on the mechanical behavior of the bone cement", *Adv. Mater. Res.*, **3**, 35-45. https://doi.org/10.12989/amr.2014.3.1.035.